Specialized ribosomes and specific ribosomal protein paralogs control translation of mitochondrial proteins

Nadav Segev and Jeffrey E. Gerst

Department of Molecular Genetics, Weizmann Institute of Science, Rehovot, Israel

Genome duplication in eukaryotes created paralog pairs of ribosomal proteins (RPs) that show high sequence similarity/identity. However, individual paralogs can confer vastly different effects upon cellular processes, e.g., specific yeast paralogs regulate actin organization, bud site selection, and mRNA localization, although how specificity is conferred is unknown. Changes in the RP composition of ribosomes might allow for specialized translation of different subsets of mRNAs, yet it is unclear whether specialized ribosomes exist and if paralog specificity controls translation. Using translatome analyses, we show that the translation of mitochondrial proteins is highly down-regulated in yeast lacking RP paralogs required for normal mitochondrial function (e.g., *RPL1b*). Although *RPL1a* and *RPL1b* encode identical proteins, Rpl1b-containing ribosomes confer more efficient translation of respiration-related proteins. Thus, ribosomes varying in RP composition may confer specialized functions, and RP paralog specificity defines a novel means of translational control.

Introduction

Translation regulation allows cells to rapidly alter their proteome in response to environmental changes and different cellular stimuli (Sonenberg and Hinnebusch, 2009; Spriggs et al., 2010), and it encompasses several layers of control. These include the interaction with ribosome-associated proteins (Fleischer et al., 2006), binding and recognition of mRNA motifs (Wilkie et al., 2003; Xue et al., 2015), mRNA localization (Kraut-Cohen et al., 2013; Buxbaum et al., 2015; Lesnik et al., 2015), and translation initiation (Sonenberg and Hinnebusch, 2009).

Although ribosomes were once conceptualized as uniform, fixed molecular machines that perform translation, it is now known that structural variations generate ribosome heterogeneity. For example, ribosomal RNA and ribosomal proteins (RPs) differ in their modification and composition within ribosomes to affect translation (Byrgazov et al., 2013; Ferretti et al., 2017; Shi et al., 2017). In yeast, 59 of the 79 RPs are encoded by paralog pairs and, although a pair may display high sequence identity, the deletion of a specific paralog can lead to phenotypes in actin regulation (Haarer et al., 2007), sporulation (Enyenihi and Saunders, 2003), bud site selection (Ni and Snyder, 2001), and mRNA localization (Komili et al., 2007). A paralog specificity model called the "ribosome code" suggests that different RP paralogs may regulate specific physiological processes. Thus, distinct subpopulations of ribosomes (i.e., specialized ribosomes) that vary in RP paralog composition might reside within cells (Komili et al., 2007). These subpopulations might promote the translation of finite sets of mRNA and therefore yield specific translational patterns (Filipovska and Rackham, 2013).

Respiratory-deficient yeast mutants fail to grow on nonfermentable carbon sources (e.g., glycerol) and form small colonies on fermentable carbon sources (e.g., glucose; Day, 2013). Four strains bear mutations in nuclear-encoded RPs: Rpl1b, Rpl2b, Rps11a, and Rps26b (Dimmer et al., 2002; Steinmetz et al., 2002; Merz and Westermann, 2009). Importantly, each paralog has an identical or near-identical copy in the genome that shows no deficiencies in respiration when mutated. Thus, RP paralogs exhibit functional differences in a manner that remains unknown.

To determine whether RP paralogs generate specialized ribosomes that shape the cellular translatome, we characterized the respiratory-deficient RP paralog mutants with respect to translational regulation. We found that specific paralogs (Rpl1b, Rpl2b, and Rps26b) are required for proper mitochondrial morphology and function. Moreover, translatome mapping using a nascent chain sequencing approach (puromycin-associated nascent chain proteomics; PUNCH-P; Aviner et al., 2014) showed that the *rpl1b*Δ translatome is distinct from respiratory-competent *rpl1a*Δ cells, the former being deficient in the production of mitochondrial and cell wall proteins. This suggests that RP paralogs play a crucial role in translational control and, in the case of Rpl1b, directly affect mitochondrial function and cell wall integrity. The ability of specific RP paralogs to favor

Correspondence to Jeffrey E. Gerst: jeffrey.gerst@weizmann.ac.il

Abbreviations used: GO, gene ontology; mMP, mRNA encoding mitochondrial protein; MS, mass spectrometry; mtsRFP, mitochondria-localized RFP; PCA, principle components analysis; PUNCH-P, puromycin-associated nascent chain proteomics; qRT-PCR, quantitative real-time PCR; RP, ribosomal protein; RT, reverse transcription; TMRE, tetramethylrhodamine ethyl ester; TPI, total proteins identified; YPD, yeast peptone dextrose.

The Rockefeller University Press
J. Cell Biol. Vol. 217 No. 1 117–126
https://doi.org/10.1083/jcb.201706059

the translation of a subset of mRNAs reveals a novel layer of translational regulation.

Results and discussion

The *pet* phenotype is observed in specific RP paralog mutants

Yeast petite (*pet*) mutants form small colonies on fermentable carbon sources (e.g., glucose) and show little or no growth on nonfermentable carbon sources (e.g., glycerol). Of these, *RPL1b*, *RPL2b*, *RPS11a*, and *RPS26b* were identified as RP paralog genes necessary for normal respiratory growth. Three paralog pairs (*RPL1a/b*, *RPL2a/b*, and *RPS11a/b*) are encoded by identical ORFs, and the fourth (*RPS26a/b*) shows a high degree of similarity. To validate the contribution of each paralog to respiratory growth, we created new deletion mutants of *RPL1b, RPL2b, RPS11a,* and *RPS26b* as well as their corresponding paralogs. We examined growth of the different RP mutants on glucose-containing yeast peptone dextrose (YPD) and glycerol-containing YPGly medium at 30°C and 35°C and found that three (*rpl1bΔ*, *rpl2bΔ*, and *rps26bΔ*) displayed the *pet* phenotype (Fig. 1 a). We measured replication times of the deletion mutants in YPD and YPGly at 30°C (Fig. 1 b) and observed that although *rpl1aΔ*, *rpl2aΔ*, and *rps26aΔ* mutant strains grow similar to WT cells, their corresponding *a* paralog mutants showed longer replicative times, especially on glycerol. However, the replication times of RP paralog pair deletions (e.g., *rpl1aΔ/bΔ* cells) showed no additive effects upon growth (Fig. S1 a). Likewise, the deletion of two respiration-related paralogs (e.g., *rpl1bΔ/2bΔ*) grew similar to single mutants (e.g., *rpl1bΔ* or *rpl2bΔ*) and did not confer more severity. Thus, the respiration-related RP paralogs act in an epistatic fashion upon the same pathway.

RPL1b, *RPL2b*, or *RPS26b* are required for normal mitochondrial function and morphology

To determine whether the slow growth phenotype of *rpl1bΔ*, *rpl2bΔ*, and *rps26bΔ* cells is caused by a specific mitochondrial impairment, we examined mitochondrial morphology and functionality in the mutants. First, we imaged mitochondria using mitochondria-localized RFP (mtsRFP) and observed that their morphology in *rpl1bΔ*, *rpl2bΔ*, and *rps26bΔ* cells appeared aggregated and less tubular, especially on glycerol (Fig. 2 a). 3D reconstruction of the mitochondria illustrates a wide range in the diversity of morphological phenotypes observed between WT and mutant cells (Fig. 2 b). Second, we determined whether RP deletions affect mitochondrial function. We measured mitochondrial inner membrane potential ($\Delta\psi$) as an indicator of functionality using tetramethylrhodamine ethyl ester (TMRE) and flow cytometry (Ludovico et al., 2001). The measured $\Delta\psi$ was exceptionally lower on glycerol for all three mutants (*rpl1bΔ*, *rpl2bΔ*, and *rps26bΔ*) when compared with their *a* paralogs of WT cells (Fig. 2 c). Analysis of the data also allowed for quantification of the changes observed in mitochondrial morphology. We calculated the mitochondrial signal/cell size ratio and found that it was lower for the respiration-deficient mutants (significantly in *rpl1bΔ* and *rps26bΔ* cells) in comparison with their corresponding paralog deletions or WT cells (Fig. S1 b). Thus, mitochondria are smaller/more aggregated in the respiration-deficient mutants, as observed visually (Fig. 2, a and b). These results indicate acute mitochondrial dysfunction and likely explain the slow growth phenotype of the *rpl1bΔ*, *rpl2bΔ*, and *rps26bΔ* cells.

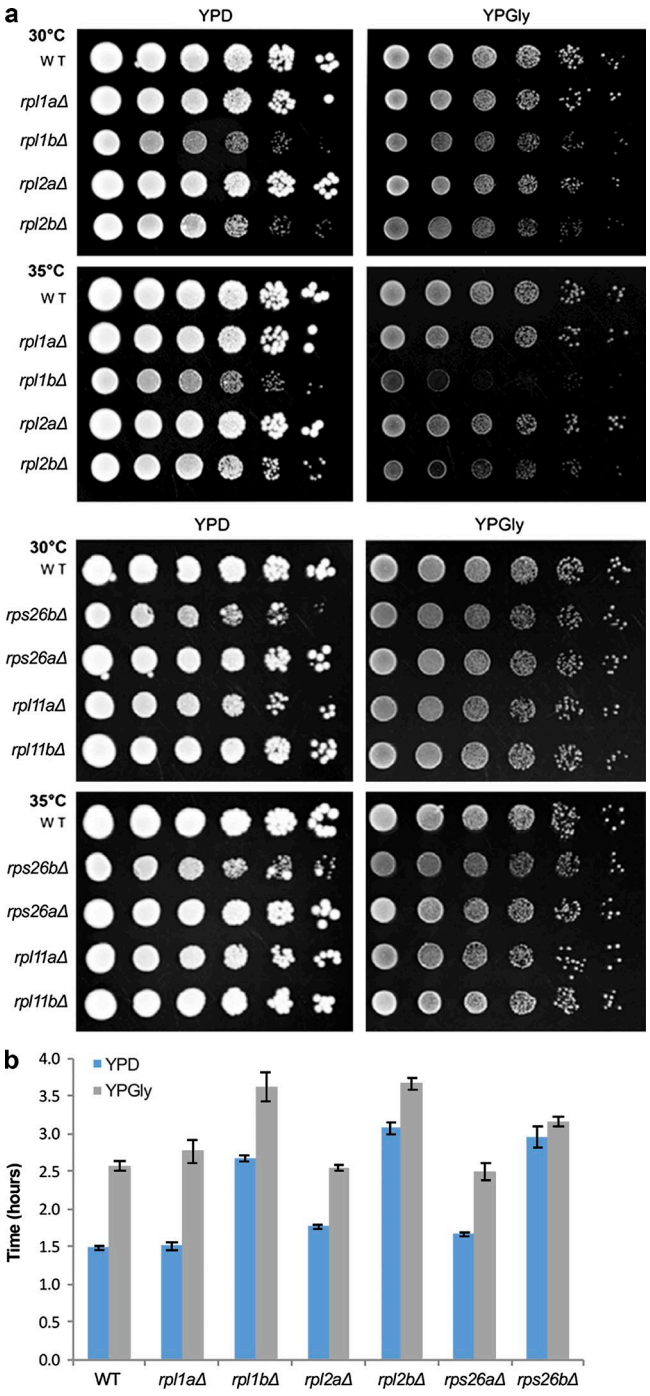

Figure 1. **Specific RP paralog mutants display *pet* phenotypes.** (a) *rpl1bΔ*, *rpl2bΔ*, and *rps26bΔ* cells grow slowly on glucose and are temperature sensitive on glycerol. WT and RP paralog deletion strains were grown to mid–log phase, serially diluted, and examined for growth on solid medium containing glucose (YPD) or glycerol (YPGly) at 30°C or 35°C. (b) *rpl1bΔ*, *rpl2bΔ*, and *rps26bΔ* cells show slower doubling times. Doubling times (in h) of the strains in panel a were obtained from growth curves of cells grown on liquid YPD or YPGly at 30°C. Error bars represent the SEM of three biological repeats.

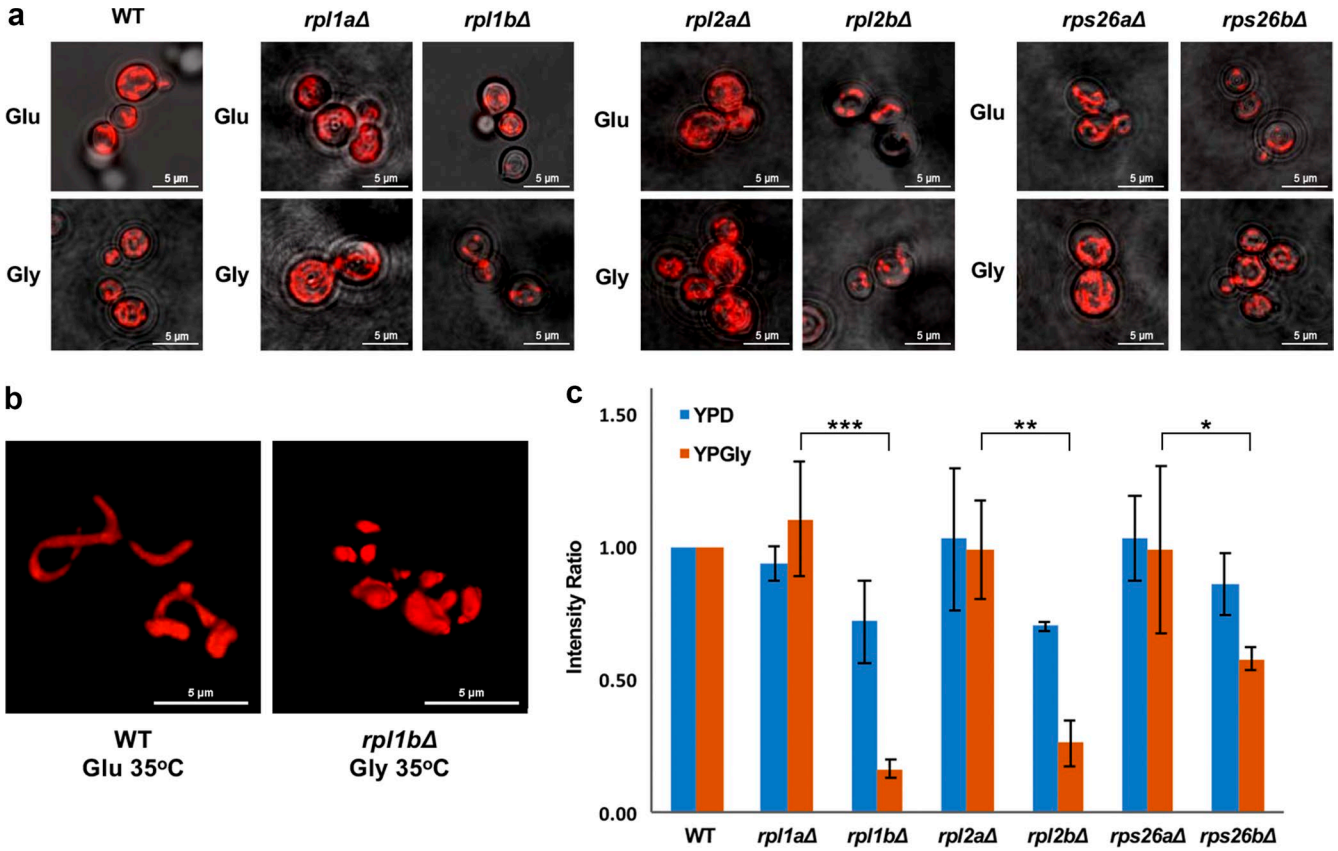

Figure 2. ***rpl1bΔ, rpl2bΔ, and rps26bΔ cells show defective mitochondrial morphology and membrane potential.*** (a) Mitochondrial morphology is altered in the *rpl1bΔ*, *rpl2bΔ*, and *rps26bΔ* mutants. WT, *rpl1bΔ*, *rpl2bΔ*, and *rps26bΔ* cells and their corresponding *a* paralog deletions expressing mtsRFP were examined for mitochondrial morphology. Cells were grown to mid–log phase on glucose (Glu; YPD) or glycerol (Gly; YPGly) at 35°C and subjected to confocal microscopy. Representative z stack images are shown. (b) Abnormal mitochondrial morphology of *rpl1bΔ* as shown by 3D visualization. Z stack images were assembled into a 3D projection of the mitochondrial morphology for the two representative phenotypes observed (i.e., normal tubular mitochondrial morphology of WT cells [left] and the aggregated morphology of *rpl1bΔ* [right]). (c) $\Delta\psi$ is reduced in the *rpl1bΔ*, *rpl2bΔ*, and *rps26bΔ* cells. WT, *rpl1bΔ*, *rpl2bΔ*, and *rps26bΔ* cells and their corresponding *a* paralog deletions were grown to mid–log phase on YPD or YPGly at 35°C. Strains were labeled with TMRE before flow cytometry, and fluorescence intensity was measured in $>10^3$ cells each using ImageStreamX and then was calculated relative to WT cells. Error bars represent SEM. *, $P \leq 0.05$; **, $P \leq 0.03$; ***, $P \leq 0.01$.

RP paralogs show functional specificity on a nonfermentable carbon source

Ribosome assembly and biogenesis is coordinated by multiple levels of regulation, including RP expression (Warner, 1999; Woolford and Baserga, 2013). For example, expression may involve different parts of the RP mRNA transcript, such as the UTRs and introns (Parenteau et al., 2011). In parallel, cognate RP paralogs were proposed to regulate the level of the other paralog's mRNA (Parenteau et al., 2015; Gabunilas and Chanfreau, 2016). However, alterations in the transcription of one paralog caused by deletion of the other do not correlate with changes in the level of RP protein (Parenteau et al., 2015; Liu et al., 2016). More importantly, RP paralogs do not show synonymous functional substitution but rather diversification. Komili et al. (2007) demonstrated that the overexpression of one RP paralog in the deletion mutant of its cognate partner may not fully complement the deletion phenotype. This finding led to the idea of paralog specificity, although there has been no firm evidence connecting paralog selectivity (in ribosomes) to changes in translation.

To verify that the *rpl1bΔ*, *rpl2bΔ*, and *rps26bΔ* phenotype is caused by paralog specificity and not a byproduct of alterations in gene expression, we measured mRNA levels of the paralogs in WT cells grown at 35°C on glucose or glycerol. The change in carbon source did not alter the *a/b* paralog expression ratio for any of the paralog pairs (Fig. 3 a).

To determine whether mutation of one RP paralog alters expression of the other, we examined the mRNA levels of each paralog upon deletion of its paralogous partner. mRNA levels of the different paralogs did not undergo noticeable changes in the absence of their cognates on YPD at 30°C, whereas increased levels of mRNA were observed for the *RPL2* and *RPS26 a* paralogs in the *b* paralog deletion strains grown on YPGly at 35°C (Fig. 3 b). Thus, the removal of one paralog may influence expression of the other, but does not necessarily confer normal cellular physiology—hence the respiration-deficient growth observed in Fig. 1.

We determined whether overexpression of a given RP paralog can complement the absence of its cognate partner. We overexpressed *a* paralogs in *b* (respiration-deficient) deletion mutants and examined their ability to grow on YPD and YPGly at 30°C and 35°C (Fig. 3 c). Plasmid-based reexpression of the *b* paralogs fully rescued deletion of their genomic copies (Fig. S2 a). In contrast, overexpression of the corresponding *a* paralogs in *rpl1bΔ*, *rpl2bΔ*, and *rps26bΔ* cells could not fully compensate for loss of the respective *b* paralogs on glycerol,

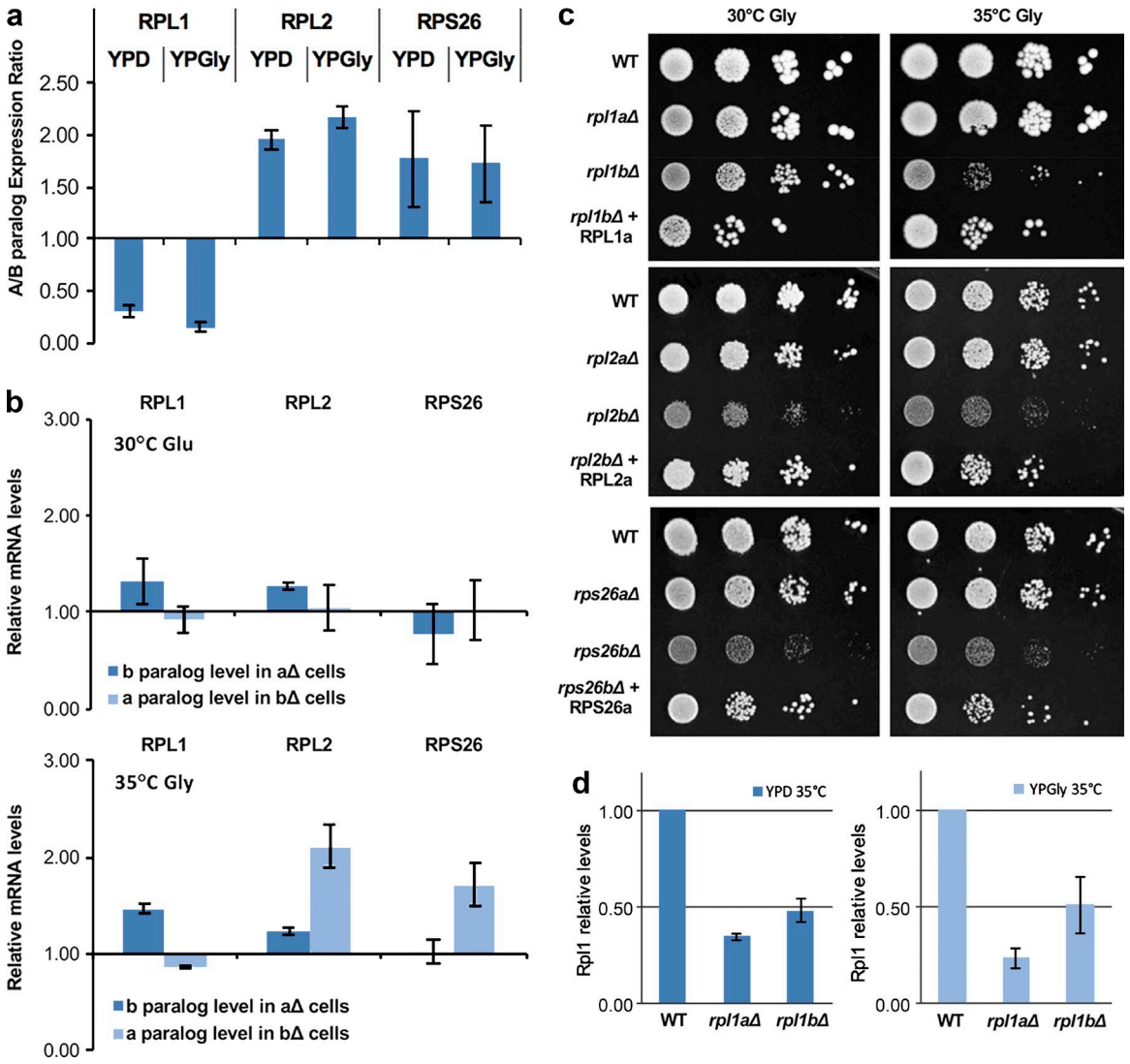

Figure 3. **RP paralog-specific phenotypes are not accompanied by changes in gene expression of the other paralog nor suppressed by its overexpression.** (a) RP paralog gene expression ratio does not change on fermentable versus nonfermentable carbon sources. WT cells were grown to mid–log phase on glucose (YPD) or glycerol (Gly; YPGly) at 35°C before RNA extraction and analysis by qRT-PCR using specific primers for each paralog. qRT-PCR experiments were performed in triplicate from three biological repeats. (b) Deletion of one RP paralog does not change expression of its cognate partner. RP deletion mutants were grown and analyzed by qRT-PCR as in panel a. Experiments were performed in triplicate from three biological repeats. mRNA levels are shown relative to WT expression. (c) Paralog overexpression only partially substitutes for the loss of its cognate partner. WT, RP deletion, and RP deletion strains overexpressing their corresponding *a* paralog from a single-copy plasmid were plated and grown on YPD or YPGly at 30°C and 35°C (Fig. S2). (d) Rpl1 protein levels decrease in both *rpl1aΔ* and *rpl1bΔ* mutants. WT, *rpl1aΔ*, and *rpl1bΔ* cells were grown to mid–log phase on YPD or YPGly at 35°C and processed for Western analysis. Rpl1 protein from each sample was quantified using GelQuantNet and normalized to total protein in each lane as detected by Ponceau staining (Fig. S2 c). No significant difference ($P > 0.05$) was detected between the Rpl1 levels in *rpl1aΔ* and *rpl1bΔ* cells. Western blotting and analysis was performed in triplicate from three biological repeats. Error bars represent SEM.

but did confer normal growth on glucose (Fig. S2 b). Thus, the mitochondrial deficiencies observed upon the deletion of *RPL1b*, *RPL2b*, and *RPS26b* cannot be attributed to changes in mRNA levels alone, indicating that the *a* and *b* paralogs are not fully redundant.

Lastly, we asked whether the deletion of one paralog leads to a reduction in the total protein for a given RP, which might cause ribosome misassembly (McIntosh et al., 2011). Rpl1 protein levels in *rpl1aΔ* and *rpl1bΔ* cells grown on YPD or YPGly at 35°C were measured by Western blotting and compared with WT cells (Figs. 3 d and S2 c). A similar decrease in total Rpl1 levels was detected in either the *rpl1aΔ* or *rpl1bΔ* mutant (Fig. 3 d). Thus, the deficiencies in mitochondrial function and respiration seen in *rpl1bΔ* cells cannot be explained by a general reduction in Rpl1 protein.

Translatome profiling of RP gene deletions reveals paralog specificity

We hypothesized that specific paralogs might favor the translation of mRNAs encoding mitochondrial proteins (mMPs). Therefore, we adapted PUNCH-P, a technique that allows for translatome mapping by polysome purification and nascent polypeptide chain sequencing (Aviner et al., 2013, 2014), for use in yeast. PUNCH-P incorporates biotinylated puromycin into newly synthesized polypeptides in purified polysomes, which can be isolated using immobilized streptavidin

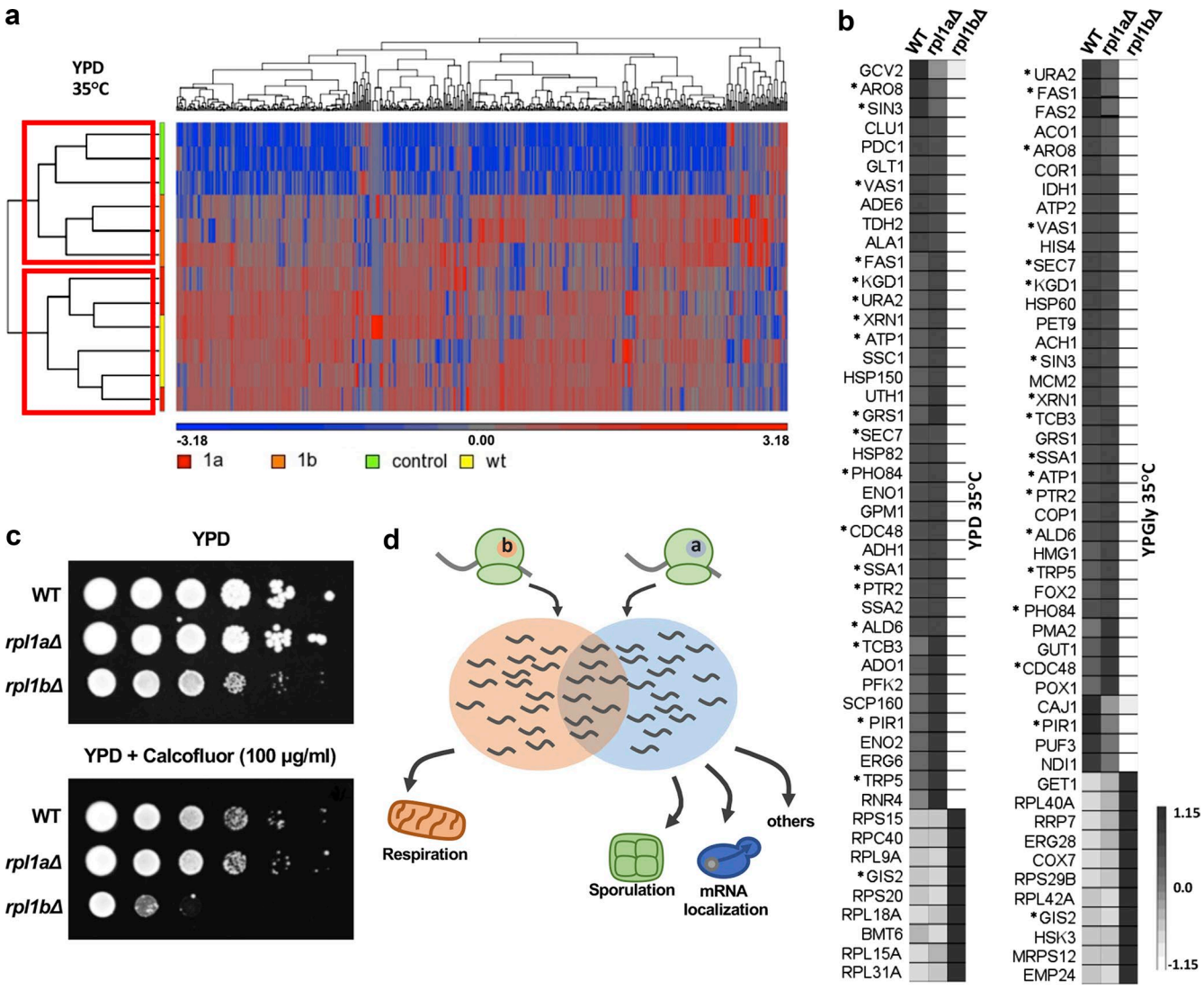

Figure 4. **Nascent chain profiling of RP deletion mutants.** (a–d) *rpl1bΔ* cells show a translatome distinct from WT and *rpl1aΔ* cells. WT, *rpl1aΔ*, and *rpl1bΔ* cells were subjected to PUNCH-P to isolate nascent polypeptide chains for MS. (a) Hierarchical clustering of the translatome profiles of cells grown on glucose (YPD) at 35°C after z score normalization ($n = 3$ biological repeats each). The repeats of *rpl1aΔ* (1a; red) and WT cells (yellow) cocluster, whereas those of *rpl1bΔ* (1b; orange) and the control samples (control; i.e., without puromycin-biotin labeling; green) cluster separately. Each cluster is statistically significant ($P < 0.05$) and is demarcated by a red rectangle. (b) Heat map of select proteins from the PUNCH-P translatome analysis of cells grown on glucose (YPD) or glycerol (YPGly) at 35°C. Representative proteins with significant change ($P \leq 0.05$) are shown after z score normalization. Asterisks indicate proteins common to both conditions. (c) *rpl1bΔ* cells are highly sensitive to cell wall stress. WT, *rpl1aΔ*, and *rpl1bΔ* strains were grown to mid–log phase on YPD, diluted serially, plated onto YPD or YPD with calcofluor (100 µg/ml), and grown at 30°C. A representative experiment ($n = 3$) is shown. (d) A general model for specialized ribosomes based on paralog specificity. Ribosomes incorporating different paralogs (i.e., the *b* paralog [pink-beige] or *a* paralog [pale blue]) translate different subsets of mRNAs relating to specific cellular processes. Thus, paralog selection determines both protein expression levels and subsequent integrity of the processes.

and the peptides analyzed by mass spectrometry (MS). We isolated translating polysomes from the *rpl1aΔ* and *rpl1bΔ* deletion mutants as well as WT controls grown at 35°C and then mapped their translatomes by MS. We identified >500 translation products from cells grown on glucose and >1,900 proteins from cells grown on glycerol (Table S1, Sheets 1 and 4, respectively).

The translatomes of the different RP paralog deletion mutants were compared by hierarchal clustering (Fig. 4 a). Although the translatomes of *rpl1aΔ* and WT cells cocluster, they are completely separate from those of *rpl1bΔ* cells or the control sample (i.e., no added biotin-puromycin; p-values <0.05). Differential clustering of the translation profiles is also seen using principle components analysis (PCA), which groups the WT and *rpl1aΔ* samples while grouping *rpl1bΔ* and the control separately (Fig. S3 a). Correlation scores for the biological repeats (Fig. S3 b: WT, $r = 0.83 \pm 0.03$; *rpl1aΔ*, $r = 0.88 \pm 0.03$; and *rpl1bΔ*, $r = 0.84 \pm 0.04$) also indicate the reproducibility of PUNCH-P. Thus, the translatome profiles are highly distinctive as a result of major changes in translation caused by the absence of a specific RP paralog (*rpl1bΔ*).

The *rpl1bΔ* translatome profile lacks mitochondria-related proteins

rpl1bΔ cells show a severe mitochondrial dysfunction phenotype (Figs. 1 and 2) and exhibit a significantly different trans-

latome profile from *rpl1aΔ* or WT cells (Fig. 4 a). To determine whether Rpl1b promotes translation of a specific subset of mRNAs (e.g., mMPs), we refined the translatome profiles from each growth condition (YPD or YPGly) to list proteins significantly missing from the *rpl1bΔ* translatome profile (Table S1; Lists 2 and 5, respectively; e.g., fold-change ≥2; P ≤ 0.05; for YPD, *n* = 54/517 of the total proteins identified [TPI] in all three strains; for YPGly, *n* = 124/1,931 TPI). More than 90% of proteins identified in the YPD translatome profile (*n* = 472/517 TPI; Table S1, List 1) were also detected in the YPGly profile (Table S1, List 4), indicating that PUNCH-P identifies proteins in a nonbiased fashion independently of growth conditions. More importantly, the refined *rpl1bΔ* translatome profile was lacking in mitochondrial proteins (Fig. 4 and Table S1, Lists 2 and 5), especially in cells grown on glycerol (Fig. 4 b, right, and Table S1, List 5). Gene ontology (GO) enrichment analysis (Huang et al., 2009) shows that ∼40% of the proteins depleted from the *rpl1bΔ* translatome in cells grown on glucose are functionally related to mitochondria (*n* = 21/54 depleted proteins; P = 2.9 E-02; Table S1, List 2). Application of the same threshold (fold change ≥2; P ≤ 0.05) for the translatome profile of cells grown on glycerol revealed a more extensive depletion of mitochondrial proteins in *rpl1bΔ* cells (*n* = 45/124; P = 3.3 E-03; Table S1, List 5). These included components of major mitochondrial pathways: tricarboxylic acid cycle (e.g., Aco1, Pck1, and Kgd1; *n* = 9/124 depleted proteins; P = 1.8 E-02); NAD/NADH cycle (e.g., Ndi1, Fox2, and Idh1; *n* = 10/124; P = 3.5 E-03); and the NADP pathway (e.g., Hmg1, Fas1, and Fas2; *n* = 11/124; P = 2.6 E-03), along with proteins having critical mitochondrial roles such as Puf3 (mRNA localization), Hsp60 (protein folding), and Por1 (porin structure; Fig. 4 b, right). Thus, the deletion of *RPL1b* results in significant changes in the translation of mMPs.

Deletion of a specific RP paralog can lead to alterations in mRNA levels (Komili et al., 2007). To determine whether changes in the translatome result from altered mMP transcription, we compared the mRNA levels of proteins that show decreased translation in the *rpl1bΔ* cells relative to *rpl1aΔ* cells. We measured the levels of various mMPs in cells grown on and glycerol by quantitative real-time PCR (qRT-PCR), but we saw no major differences in their levels of expression between the paralog mutants (Fig. S3, c and d). Accordingly, proteomic differences observed between the paralog mutants cannot be explained merely by changes in mRNA levels, but they can be attributed to differences in translation.

Translatome analysis also revealed proteins whose translation is elevated in *rpl1bΔ* cells in comparison with *rpl1aΔ* and WT cells. GO analysis of the elevated proteins showed an enrichment in proteins related to the ER (e.g., Get1, Sbh2, and Yop1; *n* = 20/85 up-regulated proteins; P = 5.8 E-04) and mitochondrial oxidative phosphorylation (e.g., Cox7, Tim11, and Atp15; *n* = 7/85; P = 7.6 E-03) in cells grown on glycerol (Fig. 4 b and Table S1, List 6). RPs (e.g., Rpl40a, Rpl29b, and Rpl42a) were found to be elevated in the *rpl1bΔ* translatome in cells grown on glycerol and, more significantly, when grown on glucose (e.g., Rps15, Rpl9a, and Rps20; *n* = 19/27 up-regulated proteins; P = 9.8 E-12; Table S1, List 3). The up-regulation of these proteins may hint at a cellular attempt to compensate for the loss of the Rpl1b paralog and may perhaps increase mitochondrial membrane potential and organelle function.

Key missing components of the *rpl1bΔ* translatome include mMPs that display respiration-deficient phenotypes when mutated, including those involved in ATP synthesis (Atp1), protein import (Scc1), tricarboxylic acid cycle (Kgd1), and other processes (Turner et al., 2000; Poirier et al., 2002; Merz and Westermann, 2009; Goswami et al., 2012). Improper translation of any or all of these proteins caused by the absence of Rpl1b likely leads to the respiration deficiency and mitochondrial defects observed. Because the partial mislocalization of a single mMP can affect mitochondrial function (Zabezhinsky et al., 2016), it is not surprising that the altered translatome of *rpl1bΔ* cells disrupts mitochondrial function and leads to the *pet* phenotype.

As the levels of *RPL1* mRNA (Fig. 3 b), mRNA translation (Table S1), and protein production (Fig. 3 d) are similar between the *rpl1aΔ* and *rpl1bΔ* mutants, changes in the translatome cannot result from a lack of Rpl1. Instead, these changes highlight differences in the functional specificity of Rpl1a and Rpl1b, proving that specific paralogs promote the translation of distinct subsets of mRNAs. Thus, not only does the RP composition of ribosomes constitute an additional layer of translational regulation (Ferretti et al., 2017; Shi et al., 2017), but paralog selectivity does as well.

Translatome profiling identifies other cellular processes governed by RP paralog specificity

Analysis of the GO profile of the *rpl1bΔ* translatome revealed reductions in other proteins not related in function to mitochondria. A significantly depleted group included cell wall components (e.g., Hsp150 and Pir1). We hypothesized then that *rpl1bΔ* mutant cells might exhibit a sensitivity to cell wall stress in comparison with *rpl1aΔ* and WT cells because of the lack of translation of these proteins. We assessed the growth of yeast exposed to calcofluor, an inducer of cell wall stress, and although WT and *rpl1aΔ* cells grew similarly, *rpl1bΔ* cells demonstrated limited growth and extreme sensitivity (Fig. 4 c). Thus, examination of the *rpl1bΔ* translatome profile led us to predict additional RP paralog-specific processes.

Identification of RNA motifs in proteins depleted in the *rpl1bΔ* translatome

Translation is mediated by different sequence elements in mRNAs (Spriggs et al., 2010; Kuersten et al., 2013). We performed computational analysis of the transcripts encoding proteins depleted in the *rpl1bΔ* translatome in an attempt to reveal motifs or similarities in sequence that might favor translation by paralog-specific ribosomes. A comparison of the codon usage in these transcripts to that of the yeast genome revealed a significant reduction in the usage of CGA and CGG codons for arginine that was observed on both glucose and glycerol (e.g., fold change ≥2; P ≤ 7.81 E-04; adjusted with Bonferroni correction; Fig. S3 e). In contrast, a moderate enrichment in GGT and GCT codons, which encode glycine and alanine, respectively, was noted in transcripts encoding proteins depleted on glucose (Fig. S3 e). Yet, no overall differences in amino acid usage in the *rpl1bΔ* translatome were noted on either carbon source. This indicates that translational control by paralog-specific ribosomes may be regulated at the RNA sequence level.

An RNA motif identification algorithm (MEME; Bailey et al., 2009) was used to identify sequence motifs in the coding region or UTRs (Mazumder et al., 2003; Wilkie et al., 2003; Berkovits and Mayr, 2015) that might facilitate paralog-specific translation. Examination of the 3′UTRs of transcripts encoding depleted proteins in the *rpl1bΔ* translatome (on glycerol) revealed a 21-nucleotide adenine-rich motif in 29/124 de-

pleted proteins (Fig. S3 f) that might potentially mediate paralog-specific interactions.

Because *RPL1a* and *RPL1b* encode the same protein at the genomic level, how might Rpl1b promote translation of a specific subset of mRNAs? One possible answer is that their different UTRs lead to differential processing of the transcripts (i.e., RNA editing) or posttranslational modifications that create distinct Rpl1 paralogs that confer altered translational control. Future studies aim to resolve the potential role of the UTRs in Rpl1 sequence identity and processing. How does Rpl1b confer altered translational control of mMPs and cell wall proteins? Although unclear, it likely acts at the different levels of translational regulation (i.e., initiation and elongation). For example, minor differences in ribosome assembly observed in *rpl1aΔ* and *rpl1bΔ* mutants suggest that Rpl1 influences translation initiation by affecting the interaction of ribosome subunits or translation factors with the translation machinery (Petitjean et al., 1995). That said, we could not identify a unique motif in the 5′UTRs that might serve as an initiation recognition site in transcripts from the *rpl1bΔ* translatome despite the recent demonstration of an RP that recognizes a particular RNA motif (Xue et al., 2015). However, specific patterns of codon usage within the coding regions (Fig. S3 d) as well as an A-rich motif in the 3′UTR of transcripts encoding proteins depleted from the *rpl1bΔ* translatome (Fig. S3 e) were identified. These factors might promote the translation of specific transcripts.

Translation is also regulated by elongation (Richter and Coller, 2015), and structural models place Rpl1 at the ribosome E site (Fei et al., 2008), which is responsible for release of the uncharged tRNAs and selectivity at the A site of tRNA entry (Wilson and Nierhaus, 2006). Importantly, the *rpl1bΔ* deletion relieves ribosome stalling at CGA arginine codons (Letzring et al., 2013), and these codons are significantly reduced in proteins of the *rpl1bΔ* translatome (Fig. S3 e). Thus, Rpl1b may connect the recognition of certain charged tRNA species (by ribosomes) to chain elongation and translational control.

In this study, we show that RP paralog specificity leads to changes in translational control (Fig. 4 d), and although the mechanism remains unclear, all three respiration-related RP paralog genes (*RPL1b*, *RPL2b*, and *RPS26a*) act epistatically (Fig. S1 a) even though they encode different subunits. Ancestral genome duplication gave rise to a large number of RP paralog gene pairs, each paralog conferring a different function from its cognate partner, despite being either identical or highly similar in amino acid sequence (Komili et al., 2007). How they act jointly to create a specialized ribosome and thus shape the translatome under differing conditions remains to be shown.

Importantly, mutated forms of ribosomal components are associated with cancer (Goudarzi and Lindström, 2016) and Diamond-Blackfan anemia, which is linked to Rps26 (Draptchinskaia et al., 1999; Ferretti et al., 2017). Future studies into the connection of RP-mediated translation of mMPs and the broader role of paralog specificity may provide a novel perspective on specialized ribosomes and translational control in human diseases.

Materials and methods

Yeast strains, genomic manipulations, and growth conditions

Cultures were grown at 30°C or 35°C in fermentable carbon source–containing media: either YPD (1% bacto–yeast extract, 2% bacto-peptone, and 2% glucose) or the nonfermentable carbon source–containing media YPGly (1% bacto–yeast extract, 2% bacto-peptone, and 3% glycerol). Synthetic selective media contained 0.67% yeast nitrogen base supplemented with ammonium sulfate, the appropriate amino acid supplements for plasmid selection, and either 2% glucose or 3% glycerol. Yeast strains used in this study are based on the BY4741 laboratory strain. Gene deletions were performed by homologous recombination using standard PCR-based amplification of deletion cassettes (Longtine et al., 1998). Standard LiOAc-based protocols were used for transformations of plasmids and PCR products into yeast.

Yeast strains included: WT cells (BY4741), *MAT*a *his3Δ1 leu2Δ0 met15Δ0 ura3Δ0*; *rpl1aΔ*, *MAT*a *his3Δ1 leu2Δ0 met15Δ0 ura3Δ0 rpl1aΔ::HIS3*; *rpl1bΔ*, *MAT*a *his3Δ1 leu2Δ0 met15Δ0 ura3Δ0 rpl1bΔ::HIS3*; *rpl2aΔ*, *MAT*a *his3Δ1 leu2Δ0 met15Δ0 ura3Δ0 rpl2aΔ::HIS3*; *rpl2bΔ*, *MAT*a *his3Δ1 leu2Δ0 met15Δ0 ura3Δ0 rpl2bΔ::HIS3*; *rps26aΔ*, *MAT*a *his3Δ1 leu2Δ0 met15Δ0 ura3Δ0 rps26aΔ::HIS3*; *rps26bΔ*, *MAT*a *his3Δ1 leu2Δ0 met15Δ0 ura3Δ0 rps26bΔ::HIS3*; *rpl1aΔ rpl2aΔ, MAT*a *his3Δ1 leu2Δ0 met15Δ0 ura3Δ0 rpl1aΔ::HIS3 rpl2aΔ::LEU2*; *rpl1aΔ rpl2bΔ*, *MAT*a *his3Δ1 leu2Δ0 met15Δ0 ura3Δ0 rpl1aΔ::HIS3 rpl2bΔ::LEU2*; *rpl1bΔ rpl2aΔ*, *MAT*a *his3Δ1 leu2Δ0 met15Δ0 ura3Δ0 rpl1bΔ::HIS3 rpl2aΔ::LEU2*; *rpl1bΔ rpl2bΔ*, *MAT*a *his3Δ1 leu2Δ0 met15Δ0 ura3Δ0 rpl1bΔ::HIS3 rpl2bΔ::LEU2*; *rpl1aΔ rps26aΔ*, *MAT*a *his3Δ1 leu2Δ0 met15Δ0 ura3Δ0 rpl1aΔ::HIS3 rps26aΔ::LEU2*; *rpl1aΔ rps26bΔ*, *MAT*a *his3Δ1 leu2Δ0 met15Δ0 ura3Δ0 rpl1aΔ::HIS3 rps26bΔ::LEU2*; *rpl1bΔ rps26aΔ*, *MAT*a *his3Δ1 leu2Δ0 met15Δ0 ura3Δ0 rpl1bΔ::HIS3 rps26aΔ::LEU2*; *rpl1bΔ rps26bΔ*, *MAT*a *his3Δ1 leu2Δ0 met15Δ0 ura3Δ0 rpl1bΔ::HIS3 rps26bΔ::LEU2*; *rpl2aΔ rps26aΔ*, *MAT*a *his3Δ1 leu2Δ0 met15Δ0 ura3Δ0 rpl2aΔ::HIS3 rps26aΔ::LEU2*; *rpl2aΔ rps26bΔ*, *MAT*a *his3Δ1 leu2Δ0 met15Δ0 ura3Δ0 rpl2aΔ::HIS3 rps26bΔ::LEU2*; *rpl2bΔ rps26aΔ*, *MAT*a *his3Δ1 leu2Δ0 met15Δ0 ura3Δ0 rpl2bΔ::HIS3 rps26aΔ::LEU2*; and *rpl2bΔ rps26bΔ*, *MAT*a *his3Δ1 leu2Δ0 met15Δ0 ura3Δ0 rpl2bΔ::HIS3 rps26bΔ::LEU2*.

Growth tests

For drop tests, serial dilutions (10-fold) of the different strains in growth medium were performed before plating by drops onto YPD and YPGly or selective minimal media containing 2% glucose or 3% glycerol at 30°C or 35°C. Plates containing the fermentable or nonfermentable carbon source were photodocumented after 2–3 d or 3–5 d, respectively. For growth curves, doubling times were calculated based on measured growth of the different strains in liquid YPD or YPGly at 30°C. Growth was assessed by OD_{600} measurements every 45 min until stationary phase. Each strain was measured for growth in triplicate and scored in three biological experiments.

Plasmids

Plasmids created for this study were constructed by restriction-free cloning (Unger et al., 2010) and verified by DNA sequencing. RP genes were cloned into pUG316 *CEN* plasmids, which contain the *URA3* selection marker, and included the coding regions (and introns in the cases of *RPL2* and *RPS26*) along with both the 5′ and 3′UTRs. UTR regions were based according to Kertesz et al. (2010). RP plasmids included pUG36-RPL1A, pUG36-RPL1B, pUG36-RPL2A, pUG36-RPL2B, pUG36-RPS26A, and pUG36-RPS26B. A multicopy *URA3* expression plasmid, pRS416-MTS-RFP, expressing *MTS-RFP* was a gift from M. Schuldiner (Weizmann Institute of Sciences, Rehovot, Israel).

Fluorescence microscopy

Yeast strains expressing mtsRFP were grown to mid-log phase (OD_{600} = 0.6–0.8) and harvested. Selective synthetic media containing fermentable (glucose) or nonfermentable (glycerol) carbon source was

used to maintain cells during photodocumentation. Cells were analyzed by fluorescence confocal microscopy. Representative images were acquired at 26°C using an LSM710 confocal microscope and a Plan Apochromat 100× 1.40 NA oil objective (ZEISS). Wavelengths for excitation at 545 nm and emission at 560–580 nm were used for the visualization of RFP in mitochondria. Image acquisition was accomplished by using the software provided by the manufacturer. Z stack projection of the fluorescence signals (Fig. 2 a) and 3D reconstructions (Fig. 2 b) were obtained using the Fiji/ImageJ (National Institutes of Health) and Volocity (PerkinElmer) programs, respectively.

ImageStreamX analysis

Yeast were grown to mid-log phase (OD_{600} = 0.6–0.8) in liquid YPD or YPGly medium at 35°C, followed by incubation with TMRE (200 nM final concentration; Biotium) for 30 min. Cells were washed once with fresh media before flow cytometry analysis. Quantitative analysis of fluorescence signals was performed by using the ImageStreamX imaging flow cytometer (Amnis; Zuba-Surma et al., 2007). Statistical analysis of ImageStreamX-collected data was performed with the IDE AS software (Amnis). Fluorescence signal intensity and area were measured for each cell examined in addition to cell size based upon differential interference contrast scattered light, which allowed for the calculation of signal intensity/area to cell size.

RNA isolation and reverse transcription (RT)/qRT-PCR analysis

RNA was extracted from each yeast strain using the MasterPure yeast RNA Purification kit (Epicentre Biotechnologies). Isolated RNA was treated with DNase (Promega) for 1.5 h at 37°C to remove contaminating DNA. RT was executed by using Moloney murine leukemia virus RT RNaseH (Promega) using conditions suggested by the manufacturer. RT reactions were performed using 1 µg RNA for each of the samples. All primer pairs produced a single amplification product (~80–120 bp) when tested by melting-curve analysis. qRT-PCR was performed using a LightCycler 480 device and CYBR Green I Master reagent (Roche). The thermocycling profile included an initial denaturation for 5 min at 95°C; 45 cycles of amplification, denaturation at 95°C for 10 s, annealing at 58°C for 20 s, and elongation at 72°C for 20 s with a single fluorescence measurement after each cycle. All sets of reactions were conducted in triplicate, and each included a negative control (without template). Crossing points for each transcript were determined using the second derivative maximum analysis with an arithmetic baseline adjustment. As *ACT1* mRNA levels are altered upon changes in cellular growth conditions, the levels of specific mRNA from each extract were normalized to the levels of *UBC6* as a control (Teste et al., 2009). The following primers were used for the detection of the different genes: qRT_RPL1a forward, 5′-CAGTCAACCAGTCGTCCAAA-3′; qRT_RPL1 reverse, 5′-TAGTTCGACGGTTTCCAAGAAG-3′; qRT_RPL1b forward, 5′-CCTCACGGACCACCAAATAC-3′; qRT_RPL2a forward, 5′-CGTAATGGCGCAATGTCATC-3′; qRT_RPL2 reverse, 5′-GAACCAGCACCCTTTCTTTG-3′; qRT_RPL2b forward, 5′-GGGTTCTGTCGCTTTGAATG-3′; qRT_RPS26a forward, 5′-AGTCAGATCCAGAGAAGACAGA-3′; qRT_RPS26a reverse, 5′-CCTTCTTGGCGGCATCA-3′; qRT_RPS26b forward, 5′-GAAGACAGAAAGAACAGAGCT-3′; qRT_RPS26b reverse, 5′-TCAGCGAGCGTTTGATTTA-3′; qRT_ACO1 forward, 5′-GCTGATGCCGTTGATGTTATG-3′; qRT_ACO1 reverse, 5′-AGTCCAACCGTTCATCTTACC-3′; qRT_ALA1 forward, 5′-GATGACGCTGCTGAGTTTAATG-3′; qRT_ALA1 reverse, 5′-TGTCACCGACAGACAACTTAC-3′; qRT_ARO8 forward, 5′-ACGCTGATGGTATCATTCCTG-3′; qRT_ARO8 reverse, 5′-GGCCCGTTGGAATAGTGTATAA-3′; qRT_ATP1 forward, 5′-TGCAAGGTCCACACCATATC-3′; qRT_ATP1 reverse, 5′-TCACAGCTTCCACGTCATTAG-3′; qRT_CDC48 forward, 5′-CGTCGTTGCTCAGGATACTATT-3′; qRT_CDC48 reverse, 5′-ATCATCGTAACCCACCTCATTC-3′; qRT_GCV2 forward, 5′-TCTGGACTGCGGAAGAAATC-3′; qRT_GCV2 reverse, 5′-CGATGTAGGTCTTCTGGTCATC-3′; qRT_KGD1 forward, 5′-TGGGCAGGGTGTTGTTTAT-3′; qRT_KGD1 reverse, 5′-GTGAATCCGATCTGGTTGTTTG-3′; qRT_LYS2 forward, 5′-CGACATCAACCGCACTTCTA-3′; qRT_LYS2 reverse, 5′-AAGACACCCATCACACATACC-3′; qRT_MCM2 forward, 5′-AAGCCATCCTGGCACTATTT-3′; qRT_MCM2 reverse, 5′-CGGAGTGAATACGGGCATAAT-3′; qRT_PUF3 forward, 5′-CATTGCTGGTCCCGTTTACTA-3′; qRT_PUF3 reverse, 5′-GTTCCCTTGTACCGTCAATCA-3′; qRT_RNR4 forward, 5′-GACCCTAAGAACATCCCTCTATTC-3′; qRT_RNR4 reverse, 5′-CAAGCTGTCATCGTTGGAAATC-3′; qRT_UBC6 forward, 5′-AACCACCGGCTATCAGAATG-3′; qRT_UBC6 reverse, 5′-TTCCAAGTATCAGGGTGGTAATC-3′; qRT_XRN1 forward, 5′-AGGGTACAGTTGTTGGCTATAC-3′; and qRT_XRN1 reverse 5′-ATCAAGCCCTAAGCCTCTATTC-3′.

Western blotting

Cell lysis, protein extraction, and Western blotting were performed as described previously by Dobzinski et al. (2015). In brief, equal amounts of protein (25 µg) from WT, *rpl1aΔ*, and *rpl1bΔ* lysates were electrophoresed on 12% polyacrylamide gels and electroblotted onto nitrocellulose blotting membranes (BioTrace; Pall Corporation). Blots were blocked with 5% BSA in PBS solution and then probed overnight at 4°C with rabbit anti-L1 antibodies (a gift from F. Lacroute, Center for Molecular Genetics, Gif-sur-Yvette, France). Secondary antibodies used for detection included horseradish peroxidase–conjugated anti–rabbit antibodies, and proteins were measured using an ECL detection kit (GE Healthcare). Results were normalized to total protein levels to avoid unsurmised fluctuations in any single protein. Total protein for each sample was quantified using Ponceau (Sigma-Aldrich) staining along the length of the whole lane. Quantification of the Ponceau-stained lanes and bands corresponding to Rpl1 was performed using GelQuant software provided by BiochemLabSolutions.com.

PUNCH-P

Polysome purification was adapted from a previously described protocol (Lesnik et al., 2014). In brief, yeast strains were grown in 800 ml of YPD or YPGly at 35°C to mid-log phase (OD_{600} = 0.6–0.8). Cells were then washed once in ice-cold double-distilled water, pelleted, and frozen. Yeast pellets were suspended in polysome extraction buffer (PEB; 20 mM Tris-HCl, pH 7.4, 10 mM $MgCl_2$, 140 mM KCl, 0.5 mM DTT, 1.4 µg/ml pepstatin, 2 µg/ml leupeptin, 40 U/ml RNAsin, 0.2 mg/ml heparin [Sigma-Aldrich], EDTA-free complete protease inhibitor mix according to manufacturer instructions [Roche], and 1% Triton X-100), and lysed using glass beads (0.4–0.6 mm). Samples were centrifuged at 17,400 *g* for 30 min at 4°C to remove cell debris before loading the 6 ml supernatant on top of 2.5 ml 70% sucrose cushion. Samples were then centrifuged in a 70.1 Ti ultracentrifuge rotor (Beckman Coulter) at 330,000 *g* for 105 min at 4°C. The pelleted polysomes were resuspended in 90 µl PEB (without detergent) and frozen in liquid nitrogen immediately. Puromycin–biotin labeling of polypeptide nascent chains and purification of the newly synthesized polypeptides from yeast polysomes was performed using by adapting the method used by Aviner et al. (2014) for mammalian polysomes. Yeast polysome concentration was determined by measuring RNA absorption at 254 nm. For each sample, 15 OD_{254} U of polysomes were incubated with 100 pmol of puromycin–biotin (Jena Bioscience) per OD_{254} U for 15 min at 37°C. Next, the samples were incubated in an overnight incubation with 5 µl of streptavidin beads (GE Healthcare) per OD_{254} U at 23°C. Beads were then resuspended with SDS–urea buffer (50 mM Tris-HCl, pH 7.5, 8 M urea, 2% [wt/vol] SDS, and 200 mM NaCl), incubated for 30 min at 23°C, and then washed five

times with 1 ml SDS–urea buffer. After this, samples were incubated with 1 M NaCl for 30 min at 23°C before washing five times in ultrapure water. Samples from three biological replicate experiments derived from each strain were subjected to MS, and peptide quantification was performed using label-free proteomics using MS1-based peptide intensity (Shalit et al., 2015). Protein quantification was inferred using the Hi-3 method (Silva et al., 2006), and the sum of the three most abundant peptides was used to calculate protein intensity in each sample.

Statistical analyses

Principle components, hierarchical clustering, and three-way ANOVA tests were performed and plotted using Partek software (Partek Inc.). Hierarchical clustering p-values were computed with multiscale bootstrap resampling using the pvclust R computing package (Suzuki and Shimodaira, 2006). ANOVA test p-values were adjusted for the false discovery rate (step-up p-value; Benjamini and Hochberg, 1995).

GO enrichment representation was analyzed by using the Database for Annotation Visualization and Integrated Discovery (DAVID; Huang et al., 2009). A Perl-based script was used to perform a permutation test for amino acid and codon usage in the genes of depleted proteins from the *rpl1bΔ* translatome. RNA motif search and identification was performed by MEME suites (Bailey et al., 2009).

Online supplemental material

Fig. S1 a shows the doubling times of the different RP paralog single- and double-deletion mutants grown on different carbon sources, and Fig. S1 b shows the quantification of mitochondrial morphology by flow cytometry. Fig. S2 a shows the growth of the *b* paralog mutants overexpressing their corresponding *a* paralog; Fig. S2 b shows the growth of the *b* paralog mutants overexpressing the *b* paralog as control; and Fig. S2 c shows the detection of Rpl1 in WT, *rpl1aΔ*, and *rpl1bΔ* cells by Western blotting; Fig. S3 a shows the similarity and grouping of the WT, *rpl1aΔ*, and *rpl1bΔ* PUNCH-P translatome profiles by PCA; Fig. S3 b shows the correlation of biological repeats obtained using PUNCH-P. Fig. S3 (c and d) show the mRNA levels of various genes coding for proteins depleted in the *rpl1aΔ* and *rpl1bΔ* translatomes relative to WT cells; Fig. S3 e shows the codon frequency of proteins depleted from the *rpl1bΔ* translatome relative to WT cells; Fig. S3 f lists genes encoding proteins depleted from the *rpl1bΔ* translatome relative to WT cells that contain an A-rich RNA motif in their 3′UTR. Table S1 provides PUNCH-P translatome profiles from each growth condition (YPD, List 1; and YPGly, List 4) for the WT, *rpl1aΔ*, and *rpl1bΔ* strains, lists of proteins significantly missing from the *rpl1bΔ* translatome profile (YPD, List 2; and YPGly, List 5), and lists of proteins which are significantly up-regulated in the *rpl1bΔ* translatome profile (YPD, List 3; and YPGly, List 6).

Acknowledgments

We thank O. Elroy-Stein and R. Aviner for advice with PUNCH-P, Y. Levin and the Israel National Center for Personalized Medicine for MS, Z. Porat for ImageStreamX, T. Olender for bioinformatics, S. Chuartzman and M. Schuldiner for advice, and F. Lacroute for anti-L1 antibodies.

This was supported by grants from the German-Israel Foundation for Scientific Research and Development (I-1190-96.13/2012), the Minerva Foundation—Germany (71130), and Kahn Center for Systems Biology, Weizmann Institute of Science. J.E. Gerst holds the Besen-Brender Chair in Microbiology and Parasitology.

The authors declare no competing financial interests.

Author contributions: N. Segev performed the experiments, data analysis, figure preparation, and writing of the manuscript; J.E. Gerst performed data analysis, figure preparation, and writing of the manuscript.

Submitted: 11 June 2017
Revised: 19 September 2017
Accepted: 17 October 2017

References

Aviner, R., T. Geiger, and O. Elroy-Stein. 2013. Novel proteomic approach (PUNCH-P) reveals cell cycle-specific fluctuations in mRNA translation. *Genes Dev.* 27:1834–1844. https://doi.org/10.1101/gad.219105.113

Aviner, R., T. Geiger, and O. Elroy-Stein. 2014. Genome-wide identification and quantification of protein synthesis in cultured cells and whole tissues by puromycin-associated nascent chain proteomics (PUNCH-P). *Nat. Protoc.* 9:751–760. https://doi.org/10.1038/nprot.2014.051

Bailey, T.L., M. Boden, F.A. Buske, M. Frith, C.E. Grant, L. Clementi, J. Ren, W.W. Li, and W.S. Noble. 2009. MEME SUITE: tools for motif discovery and searching. *Nucleic Acids Res.* 37(Web Server):W202–W208. https://doi.org/10.1093/nar/gkp335

Benjamini, Y., and Y. Hochberg. 1995. Controlling the False Discovery Rate: A Practical and Powerful Approach to Multiple Testing on JSTOR. *J.R. Statist. Soc.* 57:289–300.

Berkovits, B.D., and C. Mayr. 2015. Alternative 3′ UTRs act as scaffolds to regulate membrane protein localization. *Nature.* 522:363–367. https://doi.org/10.1038/nature14321

Buxbaum, A.R., G. Haimovich, and R.H. Singer. 2015. In the right place at the right time: visualizing and understanding mRNA localization. *Nat. Rev. Mol. Cell Biol.* 16:95–109. https://doi.org/10.1038/nrm3918

Byrgazov, K., O. Vesper, and I. Moll. 2013. Ribosome heterogeneity: another level of complexity in bacterial translation regulation. *Curr. Opin. Microbiol.* 16:133–139. https://doi.org/10.1016/j.mib.2013.01.009

Day, M. 2013. Yeast petites and small colony variants: for everything there is a season. *Adv. Appl. Microbiol.* 85:1–41. https://doi.org/10.1016/B978-0-12-407672-3.00001-0

Dimmer, K.S., S. Fritz, F. Fuchs, M. Messerschmitt, N. Weinbach, W. Neupert, and B. Westermann. 2002. Genetic basis of mitochondrial function and morphology in Saccharomyces cerevisiae. *Mol. Biol. Cell.* 13:847–853. https://doi.org/10.1091/mbc.01-12-0588

Dobzinski, N., S.G. Chuartzman, R. Kama, M. Schuldiner, and J.E. Gerst. 2015. Starvation-Dependent Regulation of Golgi Quality Control Links the TOR Signaling and Vacuolar Protein Sorting Pathways. *Cell Reports.* 12:1876–1886. https://doi.org/10.1016/j.celrep.2015.08.026

Draptchinskaia, N., P. Gustavsson, B. Andersson, M. Pettersson, T.N. Willig, I. Dianzani, S. Ball, G. Tchernia, J. Klar, H. Matsson, et al. 1999. The gene encoding ribosomal protein S19 is mutated in Diamond-Blackfan anaemia. *Nat. Genet.* 21:169–175. https://doi.org/10.1038/5951

Enyenihi, A.H., and W.S. Saunders. 2003. Large-scale functional genomic analysis of sporulation and meiosis in Saccharomyces cerevisiae. *Genetics.* 163:47–54.

Fei, J., P. Kosuri, D.D. MacDougall, and R.L. Gonzalez Jr. 2008. Coupling of ribosomal L1 stalk and tRNA dynamics during translation elongation. *Mol. Cell.* 30:348–359. https://doi.org/10.1016/j.molcel.2008.03.012

Ferretti, M.B., H. Ghalei, E.A. Ward, E.L. Potts, and K. Karbstein. 2017. Rps26 directs mRNA-specific translation by recognition of Kozak sequence elements. *Nat. Struct. Mol. Biol.* 24:700–707. https://doi.org/10.1038/nsmb.3442

Filipovska, A., and O. Rackham. 2013. Specialization from synthesis: how ribosome diversity can customize protein function. *FEBS Lett.* 587:1189–1197. https://doi.org/10.1016/j.febslet.2013.02.032

Fleischer, T.C., C.M. Weaver, K.J. McAfee, J.L. Jennings, and A.J. Link. 2006. Systematic identification and functional screens of uncharacterized proteins associated with eukaryotic ribosomal complexes. *Genes Dev.* 20:1294–1307. https://doi.org/10.1101/gad.1422006

Gabunilas, J., and G. Chanfreau. 2016. Splicing-Mediated Autoregulation Modulates Rpl22p Expression in Saccharomyces cerevisiae. *PLoS Genet.* 12:e1005999. https://doi.org/10.1371/journal.pgen.1005999

Goswami, A.V., M. Samaddar, D. Sinha, J. Purushotham, and P. D'Silva. 2012. Enhanced J-protein interaction and compromised protein stability of mtHsp70 variants lead to mitochondrial dysfunction in Parkinson's disease. *Hum. Mol. Genet.* 21:3317–3332. https://doi.org/10.1093/hmg/dds162

Goudarzi, K.M., and M.S. Lindström. 2016. Role of ribosomal protein mutations in tumor development (Review). *Int. J. Oncol.* 48:1313–1324.

Haarer, B., S. Viggiano, M.A. Hibbs, O.G. Troyanskaya, and D.C. Amberg. 2007. Modeling complex genetic interactions in a simple eukaryotic genome: actin displays a rich spectrum of complex haploinsufficiencies. *Genes Dev.* 21:148–159. https://doi.org/10.1101/gad.1477507

Huang, D.W., B.T. Sherman, and R.A. Lempicki. 2009. Systematic and integrative analysis of large gene lists using DAVID bioinformatics resources. *Nat. Protoc.* 4:44–57. https://doi.org/10.1038/nprot.2008.211

Kertesz, M., Y. Wan, E. Mazor, J.L. Rinn, R.C. Nutter, H.Y. Chang, and E. Segal. 2010. Genome-wide measurement of RNA secondary structure in yeast. *Nature.* 467:103–107. https://doi.org/10.1038/nature09322

Komili, S., N.G. Farny, F.P. Roth, and P.A. Silver. 2007. Functional specificity among ribosomal proteins regulates gene expression. *Cell.* 131:557–571. https://doi.org/10.1016/j.cell.2007.08.037

Kraut-Cohen, J., E. Afanasieva, L. Haim-Vilmovsky, B. Slobodin, I. Yosef, E. Bibi, and J.E. Gerst. 2013. Translation- and SRP-independent mRNA targeting to the endoplasmic reticulum in the yeast Saccharomyces cerevisiae. *Mol. Biol. Cell.* 24:3069–3084. https://doi.org/10.1091/mbc.E13-01-0038

Kuersten, S., A. Radek, C. Vogel, and L.O.F. Penalva. 2013. Translation regulation gets its 'omics' moment. *Wiley Interdiscip. Rev. RNA.* 4:617–630.

Lesnik, C., Y. Cohen, A. Atir-Lande, M. Schuldiner, and Y. Arava. 2014. OM14 is a mitochondrial receptor for cytosolic ribosomes that supports co-translational import into mitochondria. *Nat. Commun.* 5:5711. https://doi.org/10.1038/ncomms6711

Lesnik, C., A. Golani-Armon, and Y. Arava. 2015. Localized translation near the mitochondrial outer membrane: An update. *RNA Biol.* 12:801–809. https://doi.org/10.1080/15476286.2015.1058686

Letzring, D.P., A.S. Wolf, C.E. Brule, and E.J. Grayhack. 2013. Translation of CGA codon repeats in yeast involves quality control components and ribosomal protein L1. *RNA.* 19:1208–1217. https://doi.org/10.1261/rna.039446.113

Liu, Y., A. Beyer, and R. Aebersold. 2016. On the Dependency of Cellular Protein Levels on mRNA Abundance. *Cell.* 165:535–550. https://doi.org/10.1016/j.cell.2016.03.014

Longtine, M.S., A. McKenzie III, D.J. Demarini, N.G. Shah, A. Wach, A. Brachat, P. Philippsen, and J.R. Pringle. 1998. Additional modules for versatile and economical PCR-based gene deletion and modification in Saccharomyces cerevisiae. *Yeast.* 14:953–961. https://doi.org/10.1002/(SICI)1097-0061(199807)14:10<953::AID-YEA293>3.0.CO;2-U

Ludovico, P., F. Sansonetty, and M. Côrte-Real. 2001. Assessment of mitochondrial membrane potential in yeast cell populations by flow cytometry. *Microbiology.* 147:3335–3343. https://doi.org/10.1099/00221287-147-12-3335

Mazumder, B., V. Seshadri, and P.L. Fox. 2003. Translational control by the 3′-UTR: the ends specify the means. *Trends Biochem. Sci.* 28:91–98. https://doi.org/10.1016/S0968-0004(03)00002-1

McIntosh, K.B., A. Bhattacharya, I.M. Willis, and J.R. Warner. 2011. Eukaryotic cells producing ribosomes deficient in Rpl1 are hypersensitive to defects in the ubiquitin-proteasome system. *PLoS One.* 6:e23579. https://doi.org/10.1371/journal.pone.0023579

Merz, S., and B. Westermann. 2009. Genome-wide deletion mutant analysis reveals genes required for respiratory growth, mitochondrial genome maintenance and mitochondrial protein synthesis in Saccharomyces cerevisiae. *Genome Biol.* 10:R95. https://doi.org/10.1186/gb-2009-10-9-r95

Ni, L., and M. Snyder. 2001. A genomic study of the bipolar bud site selection pattern in Saccharomyces cerevisiae. *Mol. Biol. Cell.* 12:2147–2170. https://doi.org/10.1091/mbc.12.7.2147

Parenteau, J., M. Durand, G. Morin, J. Gagnon, J.F. Lucier, R.J. Wellinger, B. Chabot, and S.A. Elela. 2011. Introns within ribosomal protein genes regulate the production and function of yeast ribosomes. *Cell.* 147:320–331. https://doi.org/10.1016/j.cell.2011.08.044

Parenteau, J., M. Lavoie, M. Catala, M. Malik-Ghulam, J. Gagnon, and S. Abou Elela. 2015. Preservation of Gene Duplication Increases the Regulatory Spectrum of Ribosomal Protein Genes and Enhances Growth under Stress. *Cell Reports.* 13:2516–2526. https://doi.org/10.1016/j.celrep.2015.11.033

Petitjean, A., N. Bonneaud, and F. Lacroute. 1995. The duplicated Saccharomyces cerevisiae gene SSM1 encodes a eucaryotic homolog of the eubacterial and archaebacterial L1 ribosomal proteins. *Mol. Cell. Biol.* 15:5071–5081. https://doi.org/10.1128/MCB.15.9.5071

Poirier, M.G., S. Eroglu, and J.F. Marko. 2002. The bending rigidity of mitotic chromosomes. *Mol. Biol. Cell.* 13:2170–2179. https://doi.org/10.1091/mbc.01-08-0401

Richter, J.D., and J. Coller. 2015. Pausing on Polyribosomes: Make Way for Elongation in Translational Control. *Cell.* 163:292–300. https://doi.org/10.1016/j.cell.2015.09.041

Shalit, T., D. Elinger, A. Savidor, A. Gabashvili, and Y. Levin. 2015. MS1-based label-free proteomics using a quadrupole orbitrap mass spectrometer. *J. Proteome Res.* 14:1979–1986. https://doi.org/10.1021/pr501045t

Shi, Z., K. Fujii, K.M. Kovary, N.R. Genuth, H.L. Röst, M.N. Teruel, and M. Barna. 2017. Heterogeneous Ribosomes Preferentially Translate Distinct Subpools of mRNAs Genome-wide. *Mol. Cell.* 67:71–83. https://doi.org/10.1016/j.molcel.2017.05.021

Silva, J.C., M.V. Gorenstein, G.Z. Li, J.P. Vissers, and S.J. Geromanos. 2006. Absolute quantification of proteins by LCMSE: a virtue of parallel MS acquisition. *Mol. Cell. Proteomics.* 5:144–156. https://doi.org/10.1074/mcp.M500230-MCP200

Sonenberg, N., and A.G. Hinnebusch. 2009. Regulation of translation initiation in eukaryotes: mechanisms and biological targets. *Cell.* 136:731–745. https://doi.org/10.1016/j.cell.2009.01.042

Spriggs, K.A., M. Bushell, and A.E. Willis. 2010. Translational regulation of gene expression during conditions of cell stress. *Mol. Cell.* 40:228–237. https://doi.org/10.1016/j.molcel.2010.09.028

Steinmetz, L.M., C. Scharfe, A.M. Deutschbauer, D. Mokranjac, Z.S. Herman, T. Jones, A.M. Chu, G. Giaever, H. Prokisch, P.J. Oefner, and R.W. Davis. 2002. Systematic screen for human disease genes in yeast. *Nat. Genet.* 31:400–404.

Suzuki, R., and H. Shimodaira. 2006. Pvclust: an R package for assessing the uncertainty in hierarchical clustering. *Bioinformatics.* 22:1540–1542. https://doi.org/10.1093/bioinformatics/btl117

Teste, M.-A., M. Duquenne, J.M. François, and J.-L. Parrou. 2009. Validation of reference genes for quantitative expression analysis by real-time RT-PCR in Saccharomyces cerevisiae. *BMC Mol. Biol.* 10:99. https://doi.org/10.1186/1471-2199-10-99

Turner, R.J., M. Lovato, and P. Schimmel. 2000. One of two genes encoding glycyl-tRNA synthetase in Saccharomyces cerevisiae provides mitochondrial and cytoplasmic functions. *J. Biol. Chem.* 275:27681–27688.

Unger, T., Y. Jacobovitch, A. Dantes, R. Bernheim, and Y. Peleg. 2010. Applications of the Restriction Free (RF) cloning procedure for molecular manipulations and protein expression. *J. Struct. Biol.* 172:34–44. https://doi.org/10.1016/j.jsb.2010.06.016

Warner, J.R. 1999. The economics of ribosome biosynthesis in yeast. *Trends Biochem. Sci.* 24:437–440. https://doi.org/10.1016/S0968-0004(99)01460-7

Wilkie, G.S., K.S. Dickson, and N.K. Gray. 2003. Regulation of mRNA translation by 5′- and 3′-UTR-binding factors. *Trends Biochem. Sci.* 28:182–188. https://doi.org/10.1016/S0968-0004(03)00051-3

Wilson, D.N., and K.H. Nierhaus. 2006. The E-site story: the importance of maintaining two tRNAs on the ribosome during protein synthesis. *Cell. Mol. Life Sci.* 63:2725–2737. https://doi.org/10.1007/s00018-006-6125-4

Woolford, J.L. Jr., and S.J. Baserga. 2013. Ribosome biogenesis in the yeast Saccharomyces cerevisiae. *Genetics.* 195:643–681. https://doi.org/10.1534/genetics.113.153197

Xue, S., S. Tian, K. Fujii, W. Kladwang, R. Das, and M. Barna. 2015. RNA regulons in Hox 5′ UTRs confer ribosome specificity to gene regulation. *Nature.* 517:33–38. https://doi.org/10.1038/nature14010

Zabezhinsky, D., B. Slobodin, D. Rapaport, and J.E. Gerst. 2016. An Essential Role for COPI in mRNA Localization to Mitochondria and Mitochondrial Function. *Cell Reports.* 15:540–549. https://doi.org/10.1016/j.celrep.2016.03.053

Zuba-Surma, E.K., M. Kucia, A. Abdel-Latif, J.W. Lillard Jr., and M.Z. Ratajczak. 2007. The ImageStream System: a key step to a new era in imaging. *Folia Histochem. Cytobiol.* 45:279–290.